Electrochimica Acta 196 (2016) 48–55

Contents lists available at ScienceDirect

Electrochimica Acta

journal homepage: www.elsevier.com/locate/electacta

GC electrode modified with carbon nanotubes and NiO for the simultaneous determination of bisphenol A, hydroquinone and catechol

Lorena Athie Goulart[1], Lucia Helena Mascaro[1,*]

Departamento de Química, Universidade Federal de São Carlos, C. P. 676, 13565-905 São Carlos, SP, Brazil

ARTICLE INFO

Article history:
Received 15 November 2015
Received in revised form 6 February 2016
Accepted 25 February 2016
Available online 27 February 2016

Keywords:
Multi-walled carbon nanotubes
Nickel oxide nanoparticles
Phenolics
Electrodeposition
Simultaneous determination

ABSTRACT

This work reports the electrochemical determination of bisphenol A (BPA), hydroquinone (HQ) and catechol (CC) using glassy carbon electrode (GCE) modified with multi-walled carbon nanotubes (MWCNT) and nickel oxide nanoparticles (NiO). MWCNT were functionalized with sulfonitric solution ($3H_2SO_4$:$1HNO_3$) and dispersed in dimethylformamide for the MWCNT/GCE manufacturing. The MWCNT/GCE was modified with NiO using cyclic potential in pH 4 maintained by an acetate buffer solution containing 0.008 mol L^{-1} of nickel nitrate. The concentration of the nickel solution and the number of cycles in the electrodeposition were studied. Morphological characterization of NiO/MWCNT/GCE was carried out by scanning electron microscopy and the presence of NiO was observed. The electrochemical behavior was evaluated by cyclic voltammetry and electrochemical impedance spectroscopy using BPA solution and the results were compared with those of GCE. The NiO/MWCNT/GCE presented the lowest charge transfer resistance. The electrochemical detection of BPA, HQ and CC was developed using differential pulse voltammetry. The analytical curves showed an excellent linear response and the detection limits for the simultaneous determination of BPA, HQ and CC were 2.8×10^{-8} mol L^{-1}, 2.70×10^{-8} mol L^{-1} and 5.9×10^{-8} mol L^{-1}, respectively.

1. Introduction

Bisphenol A (2,2-bis (4-hydroxyphenyl) propane) (BPA) is an organic compound used in large scale at the plastics industry and as a precursor in the synthesis of polycarbonates and epoxy resins. It is an endocrine disruptor that can mimic hormones that are directly linked to growth and to the development of the reproductive system of humans and animals. Intense exposure to this compound can lead to breast or prostate cancer, infertility, diabetes and obesity [1,2]. Due to environmental problems caused by BPA various methods have been developed for its degradation [3–5]. However, during the BPA oxidation process, reaction intermediates such as phenol, hydroquinone, *p*-benzoquinone and catechol, among others are commonly formed [6,7]. Hydroquinone (HQ) and catechol (CC) are two isomers of phenolic compounds which are important environmental pollutants due to their high toxicity and low degradability in the ecological system. Furthermore, one of the greatest problems in the determination of such isomers is that they exhibit similarities in their structure and properties and usually coexist and interfere with each other during an analytical determination [8,9]. Thus, reliable analytical methods are required for sensitive simultaneous determination of BPA and its reaction intermediates in different matrices. The electrochemical methods provide an easy and fast way in environmental analysis; these methods stand out because they present low cost, reduced analysis time, small reagent consumption and the possibility of simultaneous determination of electroactive chemical species using sensors [10]. In recent years, several nanostructured materials have been developed and applied in electrochemical studies. Nanoparticles have attracted much attention due to their high surface area, electronic, optical and catalytic properties; these particles are being used in the manufacturing of sensors [11–13]. Especially metallic nanoparticles such as gold [14–16], silver [17–19], antimony [20,21] and platinum [22,23]; as well as metal oxide nanoparticles such as ZnO [24], MnO_2 [25], NiO [26,27], CuO [28,29] and SnO_2 [30,31]. Nickel oxide nanoparticles (NiO) stood out due to their extraordinary catalytic activities, high conductivities and low cost; they are also environmentally friendly [32,33]. Several studies described

* Corresponding author. Tel.: +55 16 33518082.
E-mail addresses: lorenaathie@hotmail.com (L.A. Goulart), lmascaro@ufscar.br, lmascaro@pq.cnpq.br (L.H. Mascaro).
[1] ISE member

http://dx.doi.org/10.1016/j.electacta.2016.02.174
0013-4686/

different methods for obtaining NiO, such as ultrasound-assisted deposition [34], spray pyrolysis method [35], chemical precipitation [36], electrodeposition [32] and hydrothermal synthesis [37]. Electrodeposition is one the most effective and easiest methods for preparing metal nanostructures; in addition to synthesize metal nanoparticles on the surface of conductive materials, this method can control the size of nanoparticles prepared by changing the electrodeposition conditions [38].

The combination of multi-walled carbon nanotubes (MWCNTs) and metallic nanoparticles has been extensively studied regarding the production of electrochemical sensors, because this combination often improves the electroanalytical responses due a synergistic effect produced by the combination of the unique properties of each material.

In the present work, the simultaneous determination of HQ, CC and BPA at the NiO/MWCNT modified glassy carbon electrode (NiO/MWCNT/GCE) is reported using differential pulse voltammetry. The electrodeposition of NiO in MWCNT under different conditions was studied by cyclic voltammetry and scanning electron microscopy (FEG-SEM). The electrochemical behavior of the molecules studied was investigated by cyclic voltammetry. There was a clear separation of the HQ, CC and BPA peaks easing their simultaneous determination. Moreover, the proposed sensor presented high stability and reproducibility. The NiO/MWCNT sensor developed can be used to monitor the BPA decrease and phenolic intermediates formed during photoelectrochemical degradation of waste.

2. Experimental

2.1. Reagents

Bisphenol A, hydroquinone and catechol were purchased from Sigma-Aldrich. MWCNT samples (purity of 95%, length of 5–15 μm, diameter of 20–40 nm) were obtained from Shenzhen Nanotech Port Co., Ltd – China. Sulfuric acid was obtained from Chemis, nitric acid was obtained from Synth. Nickel nitrate was obtained from Vetec. All other chemicals were of analytical grade and used without further purification. Phosphate buffer solution (PBS) (0.1 mol L^{-1}) was prepared using NaH_2PO_4 and Na_2HPO_4 (obtained from Synth); acetate buffer solution (0.1 mol L^{-1}) was prepared using H_3CCOOH and $H_3CCOONa$ (obtained from Synth and Vetec). The pH of the buffer solutions were adjusted using NaOH (obtained from Synth). All aqueous solutions were prepared with water purified from a Millipore Milli-Q system (>18.2 MΩ).

2.2. Apparatus

Electrochemical measurements were conducted on an Autolab PGSTAT30 model (Eco Chemie, Utrecht, Netherlands) potentiostat/galvanostat, controlled by GPES 4.9 software (Eco Chemie). A conventional three-electrode cell was used with: bare or modified GCE (5.0 mm diameter) as the working electrode, Ag/AgCl (KCl 3.0 mol L^{-1}) as the reference electrode and platinum as the counter electrode. Cyclic voltammetry (CV) experiments were carried out in a potential range from −0.2 V to +1.0 V with a scan rate of 50 mV s^{-1}. For differential pulse voltammetry (DPV) experiments, a scan rate of 10 mV s^{-1}, amplitude of 100 mV and a step potential of 2 mV were employed. Analytical curves were obtained from the addition of volumes of BPA standard solutions and the detection limit (LOD) was calculated according to the IUPAC recommendation [39]. Electrochemical impedance spectroscopy (EIS) was performed using an Autolab PGSTAT30 model (Eco Chemie, Utrecht, Netherlands) equipped with FRA2 software (Eco Chemie, Utrencht, Netherlands). The EIS measurements scanned a frequency range from 100 kHz to 0.1 Hz with amplitude of 10 mV measuring 10 data points every 10 frequency units. EIS measurements for the GCE were made applying a midpoint potential of

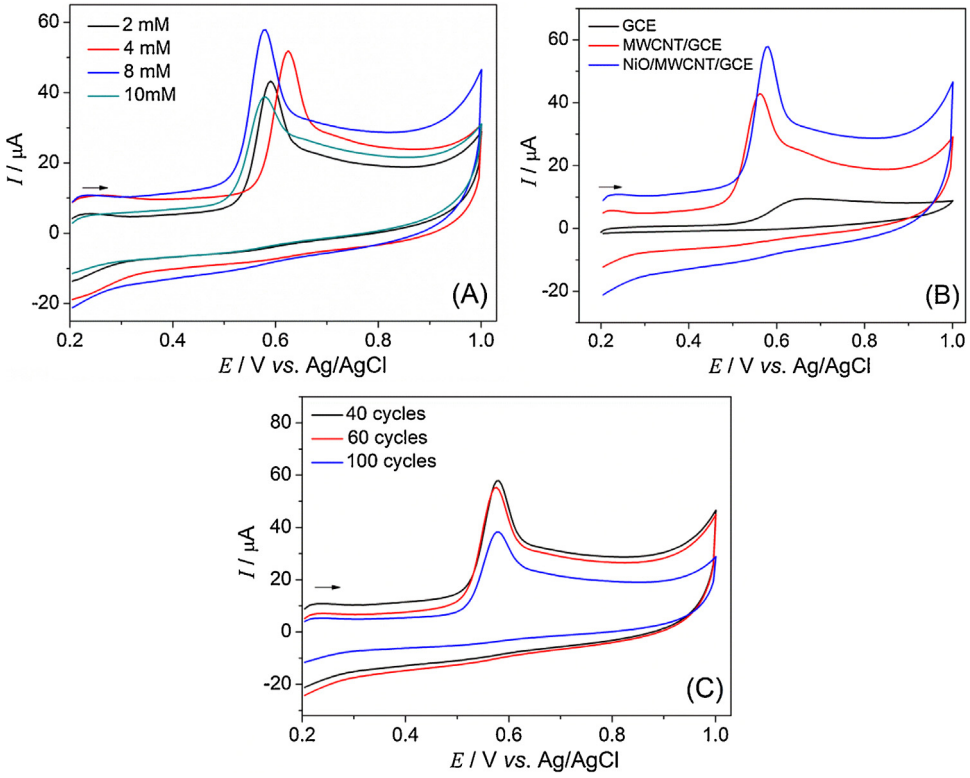

Fig. 1. Cyclic voltammograms obtained for 1.0×10^{-4} mol L^{-1} BPA in 0.1 mol L^{-1} PBS pH 6.0. (A) Effect of $Ni(NO_3)_2$ concentration in the electrodeposition of nickel oxide nanoparticles on MWCNT/GCE (2, 4, 8 and 10 mmol L^{-1}); (B) CVs for NiO/MWCNT/GCE with 8 mmol L^{-1} $Ni(NO_3)_2$ solution, MWCNT and GCE electrodes; (C) Effect of the number of cycles in the electrodeposition of nickel oxide nanoparticles on MWCNT/GCE, with 8 mmol L^{-1} $Ni(NO_3)_2$ solution.

0.6 V; for the MWCNT/GCE and the NiO/MWCNT/GCE the applied midpoint potential was 0.54 V. Scanning electron microscopy (FEG-SEM) images were obtained using scanning electron microscopy (FEG-SEM) with field emission gun; the equipment was a FEG-Zeiss model Supra 35VP (Zeiss, Germany) equipped with a higher-resolution secondary electron detector (in-lens detector), operating at 6.0 kV with a point-to-point resolution of 3.8 nm. Samples were prepared by dripping a MWCNT suspension on a glassy carbon plate. The films were dried for 12 hours.

2.3. Preparation of NiO/MWCNT/GCE

Initially, the carbon nanotubes were pre-treated in a mixture of concentrated sulfuric and nitric acids in a proportion of 3:1 v/v, respectively. This mixture was stirred for 12 hours at room temperature and was subsequently filtered, then continuously washed using purified water until pH of 6.5–7.0 was reached and then dried in an oven for 12 hours at 70 °C. This pre-treatment can lead to changes on the CNT morphology such as a sharp decrease of the tubes' diameter, unblocking of the ends of the CNT ends and the high incorporation of several functional groups, such as hydroxyl, carboxyl, epoxide and other oxygenated species [40]. After the pre-treatment, 1.0 mg of MWCNT was suspended in 1.0 mL of dimethylformamide (DMF) and this suspension was stirred in ultrasonic bath for 30 min.

Prior to modification, the bare GCE was carefully polished with 0.3 μm alumina/water mixture and then washed ultrasonically, first in ethanol and then in water during 5 minutes each. After this, the GCE was electrochemically cleaned in 0.1 mol L^{-1} pH 7.0 PBS with subsequent application of the anodic potential of +1.5 V during 60 s, followed by an application of the cathodic potential of −1.5 V during 60 s. Then, 50 cyclic voltammograms were obtained in a potential range from −1.0 V to +1.0 V, in order to obtain a reproducible and stable voltammetric behavior. The NiO/MWCNT/GCE was prepared as follows: 10 μL of the MWCNT suspension in DMF was dripped on the GCE surface followed by solvent evaporation at room temperature to form the GCE modified with MWCNT. The electrodeposition of metallic nickel was carried out using cyclic potential (40 scans between 0 and −0.8 V with a scan rate of 100 mV s^{-1}) in 0.1 mol L^{-1} acetate buffer solution (pH 4.0) containing 8 mmol L^{-1} $Ni(NO_3)_2$. After that, the potential was repeatedly cycled (40 scans between 0 and −0.65 V with a scan rate of 100 mV s^{-1}) in fresh NaOH solution for electrodissolution and passivation of a NiO layer at the MWCNT/GCE [26]. The cyclic voltammograms featuring Ni electrodeposition and the passivation of the NiO layer in NaOH solution are presented in Figure A, supporting information. For comparison, different electrode arrangements were made: NiO/GCE, MWCNT/NiO/GCE and NiO/MWCNT/GGE. The concentration of the nickel solution and the number of cycles for NiO electrodeposition were studied.

3. Results and discussion

3.1. Electrodeposition of NiO on MWCNT/GCE and morphology characterization

The electrodeposition of nickel oxide nanoparticles on MWCNT/GCE was studied using different concentrations for the $Ni(NO_3)_2$ solution: 2, 4, 8 and 10 mmol L^{-1} at pH 4.0 maintained by acetate buffer solution 0.1 mol L^{-1}. After electrodeposition, all electrodes were cycled in a fresh NaOH solution (0.1 mol L^{-1}) for electrodissolution and passivation of a nickel oxide layer at the MWCNT/GCE. The electrochemical response of different electrodes was evaluated for 1.0×10^{-4} mol L^{-1} BPA in PBS pH 6.0 using cyclic voltammetry, Fig. 1A. In this figure an anodic peak attributed to BPA oxidation was observed at approximately 0.6 V. It was observed that a increasing the concentration of the $Ni(NO_3)_2$ solution promotes an increase in the BPA oxidation current for the sensors that were deposited on 2, 4 and 8 mmol L^{-1} solution. However, a decrease of the BPA peak current (I_{pa}) is observed for NiO deposited from a 10 mmol L^{-1} $Ni(NO_3)_2$ solution. Higher I_{pa} was obtained with the NiO/MWCNT/GC electrode electroplated

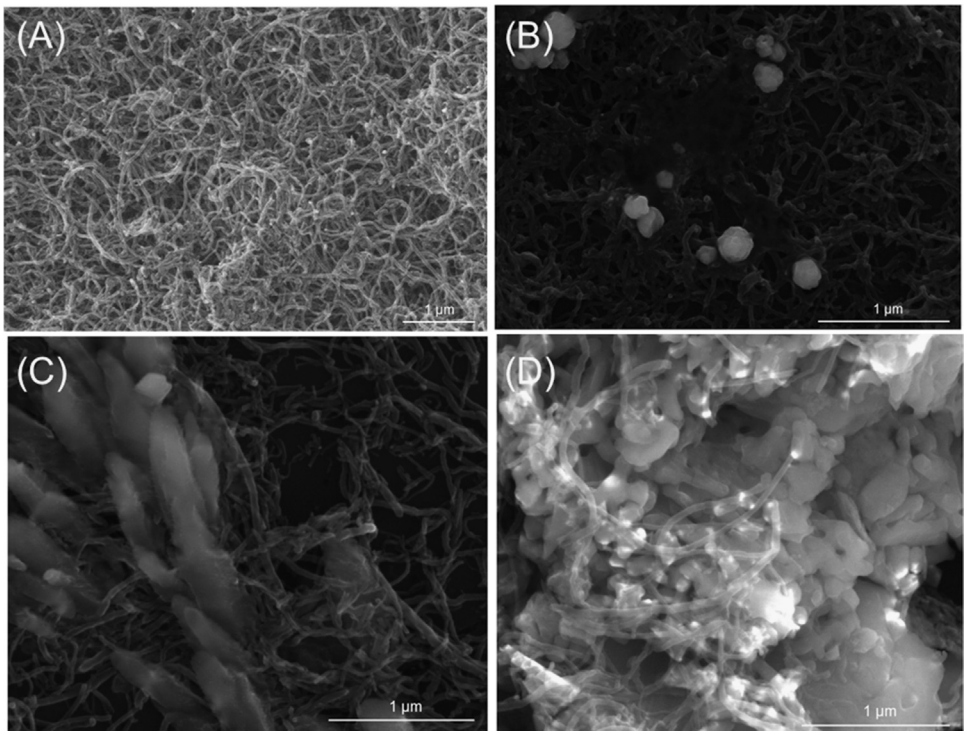

Fig. 2. SEM image of MWCNT/GCE (A), NiO/MWCNT/GCE after 40 cycles with 2 mmol L^{-1} $Ni(NO_3)_2$ (B), NiO/MWCNT/GCE after 40 (C) and 100 cycles (D) with 8 mmol L^{-1} $Ni(NO_3)_2$ solution.

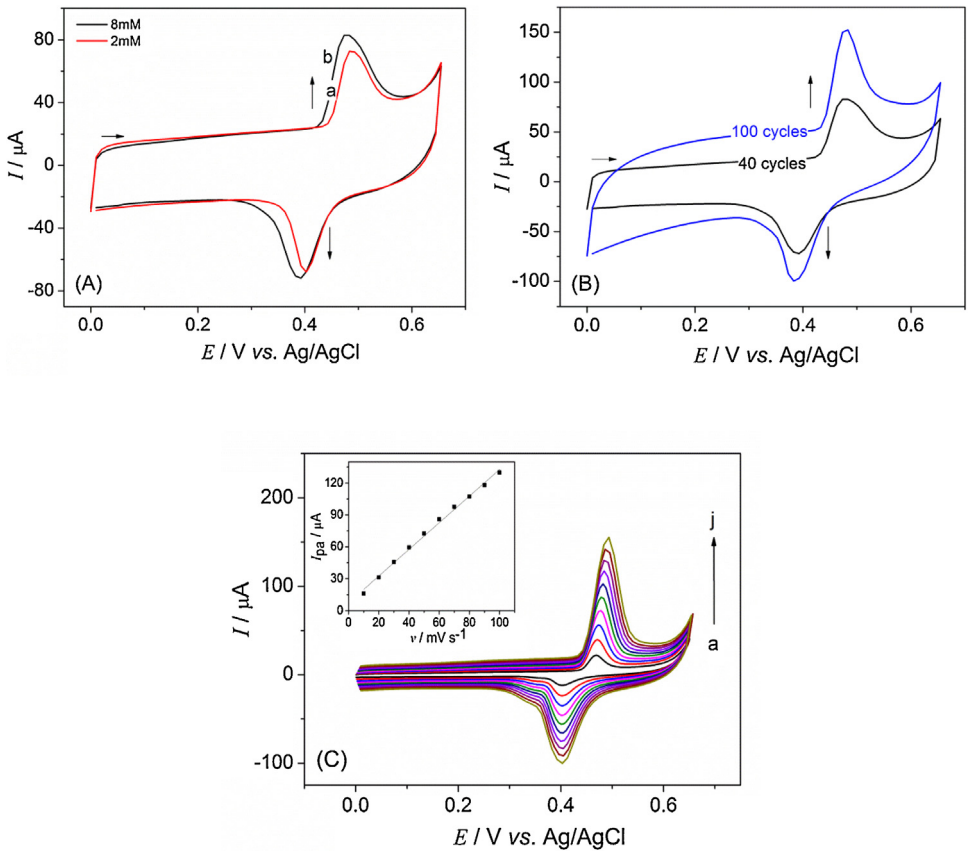

Fig. 3. Cyclic voltammetry of NiO electroplating varying the concentration of $Ni(NO_3)_2$ solution, (a) 2 mmol L^{-1} and (b) 8 mmol L^{-1} (A) and the number of cycles (40 cycles and 100 cycles) (B); Cyclic voltammograms of NiO/MWCNT/GCE in 0.1 mol L^{-1} NaOH solution at different scan rates (from *a* to *j* 10, 20, 30, 40, 50, 60, 70, 80, 90 and 100 mV s^{-1}). Inset: I_{pa} (μA) *vs.* *v* (mV s^{-1}) (C).

with an 8 mmol L^{-1} $Ni(NO_3)_2$ solution; in this case the I_{pa} is also higher when compared to the values for MWCNT/GCE and GCE, Fig. 1B. In addition, the study of the number of cycles in the NiO electrodeposition was made, in which 40, 60 and 100 cycles were studied. It was found that the increase in the number of cycles for the electrodeposition of NiO nanoparticles from 40 to 100 cycles decreased I_{pa} by 35%, Fig. 1C. As nickel oxide is deposited over the carbon nanotubes, these may be completely or partially covered, decreasing the surface area of the electrodes. Therefore, when a great amount of NiO nanoparticles is deposited, a decrease in the BPA oxidation current is observed. So, the higher I_{pa} for BPA was obtained using 40 cycles and 8 mmol L^{-1} $Ni(NO_3)_2$ solution, these experimental conditions were used to prepare the NiO/MWCNT/GC electrode for the analysis of BPA, CC and HQ.

In Fig. 2, the FEG-SEM images of MWCNTs/GCE and NiO/MWCNTs/GCE, electrodeposited from 2 and 8 mmol L^{-1} $Ni(NO_3)_2$ with different numbers of NiO growth cycles, are presented. It is observed in Fig. 2A, for MWCNTs/GCE, that carbon nanotubes are

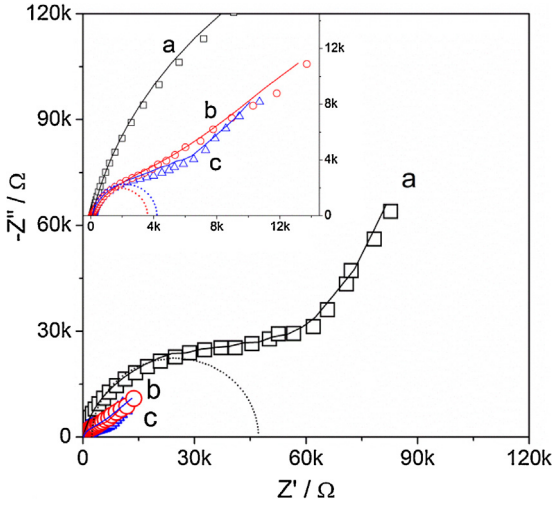

Fig. 4. Nyquist plots obtained from impedance measurements in the presence of 1.0×10^{-3} mol L^{-1} BPA in 0.1 mol L^{-1} PBS solution pH 6.0 for (a) GCE, (b) NiO/MWCNT/GCE and (c) MWCNT/GCE. Inset: magnified plots of (a), (b) and (c) at the high-frequency region.

Table 1
Charge transfer resistance (R_{ct}) for the BPA oxidation with different electrodes.

Electrodes	GCE	MWCNT/GCE	NiO/MWCNT/GCE
R_{ct} (kΩ)	45.8	4.60	3.50

distributed uniformly over the GCE surface. With the nickel oxide electrodeposition made in 2 mmol L^{-1} $Ni(NO_3)_2$ solution using 40 cycles, there was the formation of a few crystals on the carbon nanotubes, Fig. 2B. These crystals are nickel oxide nanoparticles with sizes between 50 and 300 nm. Increasing the concentration of the solution to 8 mmol L^{-1} and keeping 40 cycles, Fig. 2C, higher NiO amounts were deposited and the morphology changed. In this case, NiO nanosheets with well-established texture and structure grew perpendicularly over the CNT [41]. On the other side, in Fig. 2D, it is observed that increasing the number of cycles to 100 also results in morphological changes. Aggregated nanocrystals were produced with the formation of a rougher surface [42]. The agglomeration of nanocrystalline particles can be attributed to extremely small crystals that are formed during the cycling process. The NiO and the CNTs are well dispersed and seem to form a network [43]. This shows that the morphology and size of the NiO nanoparticles are directly related to the concentration of the $Ni(NO_3)_2$ solution and to the number of cycles used in the electrodeposition step.

The presence of nickel, oxygen and carbon in the electrodeposited film was proven by the peaks observed in the EDS analysis (Figure B in supplementary information), showing that NiO nanoparticles had successfully modified the surface of the MWCNT/GCE. The results showed a high percentage of carbon (85.0%), which can be attributed to the carbon nanotubes and glassy carbon substrate. Calculated percentages were 13.4% of oxygen and 1.0% of nickel. Besides the electrodeposition, the presence of oxygen in the CNT sample is also attributed to the previous functionalization procedure, in which hydroxyl and carboxyl groups were anchored onto the CNT surfaces [40].

The nickel oxide layer on the surface of the electrode surface is also confirmed by the electrochemical profile observed in the cyclic voltammograms for electrodes with 0.1 mol L^{-1} NaOH solution. In Fig. 3A and 3B the cyclic voltammograms of NiO/MWCNT/GCE, obtained from 2 and 8 mmol L^{-1} $Ni(NO_3)_2$ solution and 40 cycles (Fig. 3A) and also 40 and 100 deposition cycles (Fig. 3B) at 8 mmol L^{-1} $Ni(NO_3)_2$ solution, are presented.

In every voltammogram of Fig. 3, redox peaks are observed between 0.4 and 0.5 V. The oxidation peak is due to the oxidation of $Ni(OH)_2$ phase to form NiO(OH), while the reduction peak is due the reduction of NiO(OH) to form $Ni(OH)_2$ according to the following reaction [26]:

$$Ni(OH)_2 + OH^- \leftrightarrow NiO(OH) + H_2O + e$$

The peak current increases only slightly when the concentration of the $Ni(NO_3)_2$ solution increases from 2 to 8 mmol L^{-1}, indicating that after NiO deposition the electrode surface area practically does not change. However, as the number of deposition cycles increase from 40 to 100, both the capacitive and the peak current increase, Fig. 3B. This behavior may be related to larger NiO crystals deposited on MWCNT/GCE, as seen in the FEG-SEM images. So, the current related to NiO processes and the capacitive current both increase because the surface area is increased.

Considering that the BPA oxidation current was higher for the NiO/MWCNT/GCE obtained from 8 mmol L^{-1} $Ni(NO_3)_2$ solution using 40 cycles, and considering SEM results and the cyclic voltammogram in NaOH solution, subsequent experiments were carried out in these conditions.

The effect of the potential scan rate on the cyclic voltammograms of NiO/MWCNT/GCE was examined. Fig. 3C shows cyclic voltammograms obtained with scan rate in the range from 10 to 100 mV s^{-1} for the NiO/MWCNT/GCE in 0.1 mol L^{-1} NaOH solution. It was observed that the ratio between the anodic and cathodic peak currents is close to unity and that both peak currents are directly proportional to the scan rate (inset in Fig. 3C). This behavior can be related to a surface confined redox process, corresponding to a rapid conversion of the surface film without diffusion, or to a kinetically controlled reaction step. On the other hand, a shift in the peak potential occurs in the scan rates from 10 to 100 mV s^{-1}. This shift can be related to swift charge transfer kinetics over this scan rates range [26].

3.2. Characterization of NiO/MWCNT/GCE from EIS experiments

EIS experiments were performed to study the interface properties and to investigate the charge transfer resistance of GCE, MWCNT/GCE and NiO/MWCNT/GCE. The interface can be modelled using a Randles equivalent circuit, consisting of the ohmic resistance of the electrolyte (R_s), the Warburg impedance (Z_w), the electron-transfer resistance (R_{ct}) and the interfacial capacitance (C_{dl}). The impedance spectra of the (a) bare GCE, (b) NiO/MWCNT/GCE and (c) MWCNT/GCE in 1.0×10^{-3} mol L^{-1} BPA with 0.1 mol L^{-1} PBS solution at pH 6.0 are presented in Fig. 4. The Nyquist plots are composed of a semicircular part at higher frequencies corresponding to processes limited by the electron transfer and a linear portion at low frequencies resulting from processes limited by diffusion [38]. The diameter of the semicircle presents the apparent charge transfer resistance (R_{ct}) for the BPA oxidation, and the R_{ct} values are presented in Table 1. A decrease in R_{ct} can be observed following the order: bare GCE > MWCNT/GCE > NiO/MWCNT/GCE. The decrease in the R_{ct} value of the GCE when modified with MWCNTs may be related to the high surface area of the carbon nanotubes and to the presence of functional

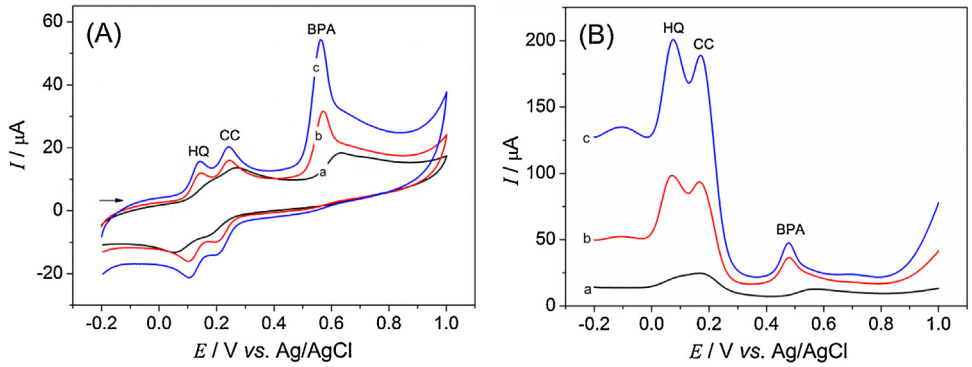

Fig. 5. (A) CV and (B) DPV of bare GCE (a), MWCNT/GCE (b) and NiO/MWCNT/GCE (c) in 0.1 mol L^{-1} PBS (pH 6.0) with 50×10^{-6} mol L^{-1} HQ, CC and BPA.

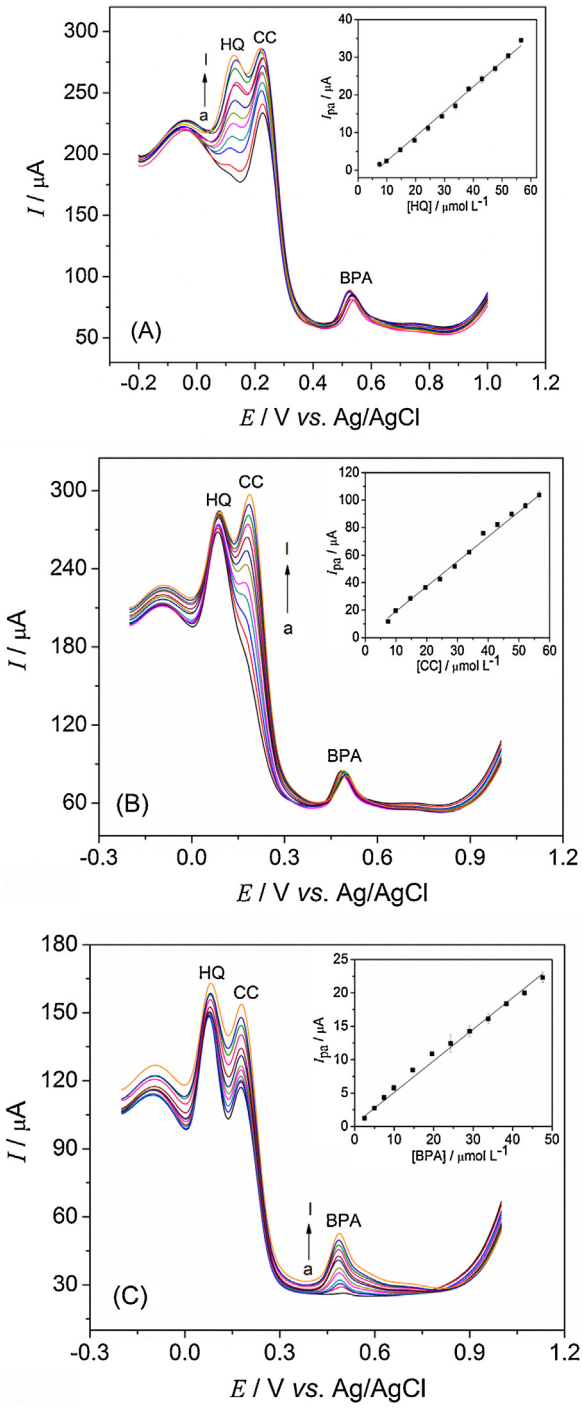

Fig. 6. (A) DPV graphs of: (a) 7.4; (b) 9.9; (c) 14.0; (d) 19.0; (e) 24.0; (f) 29.0; (g) 33.0; (h) 38.0; (i) 43.0; (j) 47.0; (k) 52.0 and (l) 56.0 µmol L^{-1} HQ in the presence of 50.0 µmol L^{-1} of CC and BPA. Inset: analytical curve for HQ. (B) DPV graphs of: (a) 7.4; (b) 9.9; (c) 14.0; (d) 19.0; (e) 24.0; (f) 29.0; (g) 33.0; (h) 38.0; (i) 43.0; (j) 47.0; (k) 52.0 and (l) 56.0 µmol L^{-1} CC HQ in the presence of 50.0 µmol L^{-1} of HQ and BPA. Inset: analytical curve for CC. (C) DPV graphs of: (a) 2.4; (b) 4.9; (c) 7.4; (d) 9.9; (e) 14.0; (f) 19.0; (g) 24.0; (h) 29.0; (i) 33.0; (j) 38.0; (k) 43.0; (l) 47.0 µmol L^{-1} BPA in the presence of 50.0 µmol L^{-1} of HQ and CC. Inset: analytical curve for BPA.

groups incorporated in the functionalization step, which enhance electrocatalytic properties [44]. After the incorporation of NiO nanoparticles on carbon nanotubes even greater decrease of R_{ct} was observed, showing that this material has good conductivity and can accelerate the electron-transfer process.

3.3. Electrochemical behavior of BPA, HQ and CC

After the BPA electrochemical behavior study and the optimization of the electrodeposition of NiO nanoparticles step, simultaneous voltammetric determination of HQ, CC and BPA was made using the NiO/MWCNT/GCE (individual behavior of HQ, CC and BPA using CV is available in the Supplementary information, Figure C). The electrochemical behavior in the blank solution (PBS 0.1 mol L^{-1}, pH 6.0) for different modified electrodes was investigated using cyclic voltammetry (CV); CV and differential pulse voltammetry (DPV) were used to investigated the electrochemical behavior in the presence of HQ, CC and BPA for different electrodes (Figure D and E, in Supplementary information). The effect of the order of the deposition of MWCNT and NiO at GCE was

Table 2
Performance comparison of the sensor proposed for detection of HQ, CC and BPA with other sensors.

Sensor	Linear range (μM)			LOD (μM)			Ref.
	HQ	CC	BPA	HQ	CC	BPA	
MnPc/MWCNT/GCE	1–600	1–600	–	0.041	0.095	–	[46]
ER(GO–TT–CNT)	0.01–200	0.5–200	–	0.007	0.011	–	[47]
PEDOT:PSS–Nafion–SWCNT-COOHs/Au	0.56–50	0.56–70	–	0.20	0.19	–	[48]
ECF-CPE	1-200	1-200	–	0.4	0.2	–	[49]
PASA/MWCNTs/GCE	6.0–100	6.0–180		1.0	1.0	–	[50]
GR/GCE	1.0–50	1.0–50	–	0.015	0.010	–	[51]
Pd@TiO_2–SiC/GCE:	0.01–200	–	0.01–200	0.005	–	0.004	[13]
PANInan./MWCNTs/PGE	–	–	1.0–400	–	–	0.001	[52]
MWCNT-GNPs/GCE	–	–	0.02–20	–	–	0.007	[53]
PGA/MWCNT-NH_2/GCE	–	–	0.1–10	–	–	0.02	[54]
Thionine-tyrosinase CPE	–	0.15–45	0.15–45	–	0.15	0.15	[55]
NiO/MWCNT/GCE	7.4–56	7.4–56	2.4–46	0.039	0.015	0.068	This work

demonstrated by comparison using HQ, CC and BPA oxidation and reduction peaks obtained by CV and DPV in 0.1 mol L^{-1} PBS (pH 6.0) containing 1.0×10^{-4} mol L^{-1} of each molecule. It was verified that higher current peaks were obtained when NiO is deposited under MWCNT. Fig. 5A and B show the CV and DPV of GCE, MWCNT/GCE and NiO/MWCNT/GCE. In Fig. 5A (a) only one broad anodic peak at about +0.26 V can be observed, which is due to the oxidation processes of HQ and CC at the GCE surface. In the reverse scan, two weak peaks appear at about +0.05 V and +0.15 V due to HQ and CC reduction processes, respectively. The BPA oxidation peak in +0.63 V, despite being separated from other peaks, is of low intensity and poor resolution. For the MWCNT/GCE three well-defined oxidation peaks were observed at +0.14, +0.24 V and +0.57 V for HQ, CC and BPA, respectively. In addition, two well-defined cathodic peaks were observed at +0.10 V and +0.20 V corresponding to the reduction of the oxidation products of HQ and CC [45]. More defined peaks and the higher peak current values were obtained with the NiO/MWCNT/GCE. Similar behavior in the oxidation processes of HQ, CC and BPA was obtained using DPV, Fig. 6B. The best results were also obtained in NiO/MWCNT/GCE, Fig. 5B (c). Thus, these results indicated that simultaneous and selective determination of HQ, CC and BPA is feasible for the NiO/MWCNT/GCE.

3.4. Simultaneous determination of HQ, CC and BPA

Individual and simultaneous determination of HQ, CC and BPA were performed using the DPV technique for the modified electrode, NiO/MWCNT/GCE. The simultaneous and individual determination of HQ, CC and BPA were first performed changing the concentration of one species and keeping the other constant. Fig. 6A shows DPV curves obtained for different concentrations of HQ in 0.1 mol L^{-1} PBS pH 6.0 and 50 μmol L^{-1} of CC and BPA. The results showed that the anodic peak current was directly proportional to the HQ concentration in the range from 7.4×10^{-6} to 5.6×10^{-5} mol L^{-1} (r = 0.995) with a detection limit (LOD) of 3.9×10^{-8} mol L^{-1} (S/N = 3). When the concentration of CC was changed and those of HQ and BPA were kept constant at 50 μmol L^{-1}, I_{pa} grew linearly with the increase of CC concentration, similarly to the HQ behavior; this is presented in the voltammograms, Fig. 6B. The linear range was from 7.4×10^{-6} to 5.6×10^{-5} mol L^{-1} (r = 0.998), and the LOD was 1.5×10^{-8} mol L^{-1} (S/N = 3). In Fig. 6C, a gradual growth in I_{pa} is observed depending on the concentration of BPA while the concentrations of HQ and CC were kept constant at 50 μmol L^{-1}. I_{pa} increases linearly with the concentration of BPA in a range from 2.4×10^{-6} to 4.6×10^{-5} mol L^{-1} (r = 0.996). The LOD for BPA was 6.8×10^{-8} mol L^{-1} (S/N = 3). A comparison of the electrode characteristics used in this work for the determination of HQ, CC and BPA with other previous literature is listed in Table 2. As can be seen, the proposed method shows good linear range, remarkable sensitivity, low detection limit and the obtained results are better than those reported in many published works [46,48–50,55]. Also, stands out the fact that is the first time that simultaneous determination of HQ, CC and BPA is reported in the literature.

Simultaneous determination of HQ, CC and BPA with NiO/MWCNT/GCE was demonstrated by changing the concentrations of the species simultaneously. As presented in Fig. 7, the differential pulse voltammograms exhibited well defined oxidation peaks at +0.08, +0.17 V and +0.48 V corresponding to HQ, CC and BPA, respectively. The oxidation peak currents of the three species increased linearly with the their concentration in the same range from 4.9×10^{-6} mol L^{-1} to 3.5×10^{-5} mol L^{-1}, with correlation coefficients of 0.997 for HQ, 0.998 for CC and 0.997 for BPA. The LOD were 2.8×10^{-8} mol L^{-1} for HQ, 2.7×10^{-8} mol L^{-1} for CC and 5.9×10^{-8} mol L^{-1} for BPA. High sensitivity was observed for determination of HQ, CC and BPA in the mixture and in individual experiments. The results show that sensitivity values are 9.4×10^{6} μA L mol^{-1}, 1.0×10^{6} μA L mol^{-1} and 5.3×10^{6} μA L mol^{-1} for HQ, CC and BPA in the mixture, respectively, and 6.5×10^{6} μA L mol^{-1}, 1.8×10^{6} μA L mol^{-1} and 4.7×10^{6} μA L mol^{-1} for pure HQ, CC and BPA, respectively. From the experiments, it was found that the NiO/MWCNT/GCE can be used for simultaneous determination of HQ, CC and BPA, since this electrode showed higher selectivity and sensitivity for the determination of the species without interference between them.

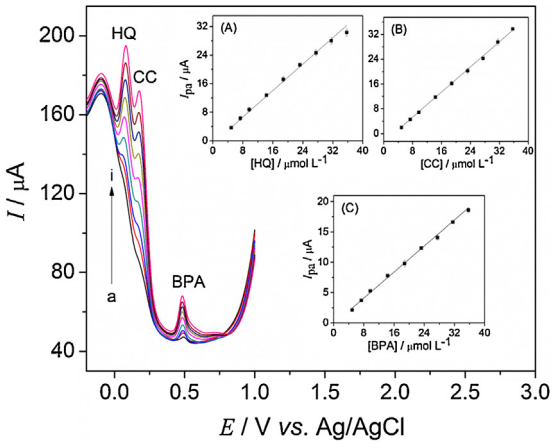

Fig. 7. Differential pulse voltammograms for various concentrations of HQ, CC and BPA in pH 6.0 PBS: (a) 4.9; (b) 7.3; (c) 9.7; (d) 14.3; (e) 18.8; (f) 23.2; (g) 27.5; (h) 31.6; (i) 35.7 μmol L^{-1}. Inset: (A) analytical curve for HQ, (B) analytical curve for CC and (C) analytical curve for BPA.

3.5. Reproducibility and stability

The reproducibility of the NiO/MWCNT/GCE was examined by the detection of 1.0×10^{-4} mol L^{-1} BPA in 0.1 mol L^{-1} PBS (pH 6.0) in three successive determinations. The relative standard deviation (RSD) was 1.75%, showing that the electrode has good reproducibility. Additionally, the NiO/MWCNT/GCE stability was also investigated. The electrode was stored in air at room temperature inside a desiccator. After 4 weeks, without any pre-conditioning treatment on the electrode, the current response was stable and kept approximately 94.6% of the originally measured value (Figure F and G, in Supplementary information). The high long-term stability and reproducibility suggested that the NiO/MWCNT/GCE is attractive to be used as an electrochemical sensor.

4. Conclusion

In this work, a simple and highly sensitive electrochemical sensor based on a modified GCE with a NiO nanoparticles and MWCNT composite film was used at simultaneous and quantitative detection of HQ, CC and BPA. The NiO/MWCNT/GCE exhibited three well defined voltammetric peaks shifted to more negative potentials with high current values compared to the peaks for the bare GCE. The NiO/MWCNT/GCE presented linear concentration range from 4.9×10^{-6} mol L^{-1} to 3.5×10^{-5} mol L^{-1}, high stability after 4 weeks and good reproducibility. Moreover, the electrode was successful in the determination of HQ, CC and BPA isolated or in a mixture of species, as they are generally found in water samples. The LOD were in the order of magnitude of 10^{-8} mol L^{-1} for HQ, CC and BPA when determined individually and simultaneously, demonstrating a great sensitivity sensor. In this way, the NiO/MWCNT/GCE is a great candidate to be used as a selective sensor for the studied species.

Acknowledgement

This work was supported by Fundação de Amparo à Pesquisa do Estado de São Paulo (FAPESP) (Process: 2012/20926-2).

Appendix A. Supplementary data

Supplementary data associated with this article can be found, in the online version, at http://dx.doi.org/10.1016/j.electacta.2016.02.174.

References

[1] J. Li, D. Kuang, Y. Feng, F. Zhang, M. Liu, Microchim Acta 172 (2011) 379.
[2] H. Fan, Y. Li, D. Wu, H. Ma, K. Mao, D. Fan, D. Bin, H. Li, Q. Wei, Anal. Chim. Acta 711 (2012) 24.
[3] D.P. Mohapatra, S.K. Brar, R.D. Tyagi, R.Y. Surampalli, Ultrasonics Sonochem. 18 (2011) 1018.
[4] V.M. Daskalaki, Z. Frontistis, D. Mantzavinos, A. Katsaounis, Catalysis Today 161 (2011) 110.
[5] R. Wang, D. Ren, S. Xia, Y. Zhang, J. Zhao, J. Hazard. Mater. 169 (2009) 926.
[6] J. Poerschmann, U. Trommler, T. Górecki, Chemosphere 79 (2010) 975.
[7] H. Katsumata, S. Kawabe, S. Kaneco, T. Suzuki, K. Ohta, J. of Photochem. and Photob. A: Chem. 162 (2004) 297.
[8] H. Du, J. Ye, J. Zhang, X. Huang, C. Yu, J. of Electroan. Chem. 650 (2011) 209.
[9] Q. Guo, J. Huang, P. Chen, Y. Liu, H. Hou, T. You, Sensors and Actuators B 163 (2012) 179.
[10] D. Zhao, X. Zhang, L. Feng, L. Jia, S. Wang, Colloids and surfaces B: Biointerfaces 74 (2009) 317.
[11] A.C. Oliveira, L.H. Mascaro, Int. J. Electrochem. Sci. 6 (2011) 804.
[12] L. Yang, H. Zhao, S. Fan, B. Li, C. Li, Analytica Chimica Acta 852 (2014) 28.
[13] A. Wang, Y. Wei, C. Wang, J. of Analytical Chemistry 70 (2015) 67.
[14] X. Niua, W. Yanga, G. Wang, J. Rena, H. Guoa, J. Gaoa. Electrochim. Acta 98 (2013) 167.
[15] L. Zhou, J. Wang, D. Li, Y. Li, Food Chemistry 162 (2014) 34.
[16] K. Huanga, Y. Liua, Y. Liua, L. Wang, J. of Hazardous Materials 276 (2014) 207.
[17] J. Tashkhourian, M.R.H. Nezhad, J. Khodavesi, S. Javadi, J. Electroanal. Chem. 633 (2009) 85.
[18] B. Liu, T. Wang, C. Yin, Z. Wei, J. Mater. Sci. 49 (2014) 5398.
[19] I. Cesarino, V. Cesarino, F.C. Moraes, T.C.R. Ferreira, M.R.V. Lanza, L.H. Mascaro, S.A.S. Machado, Materials Chemistry and Physics 141 (2013) 304.
[20] F.C. Moraes, I. Cesarino, V. Cesarino, L.H. Mascaro, S.A.S. Machado, Electrochimica Acta 85 (2012) 560.
[21] I. Cesarino, V. Cesarino, M.R.V. Lanza, Sensors and Actuators B 188 (2013) 1293.
[22] Z. Zheng, Y. Du, Z. Wang, Q. Feng, C. Wang, Analyst 138 (2013) 693.
[23] P.D. Marreto, A.B. Trench, F.C. Vicentini, L.C.S. Figueiredo-Filho, R.A. Medeiros, E.C. Pereira, O. Fatibello-Filho, Australian journal of Chemistry 68 (2015) 800.
[24] L. Jiang, S.Q. Gu, Y.P. Ding, F. Jiang, Z. Zhang, Nanoscale 6 (2013) 207.
[25] S.Q. liu, T.X. Luo, L. Li, Instrum. Sci. Technol. 41 (2013) 382.
[26] M. Roushani, M. Shamsipur, S.M. Pourmortazavi, J. Appl. Electrochem. 42 (2012) 1005.
[27] L.C.S. Figueiredo-Filho, T.A. Silva, F.C. Vicentini, O. Fatibello-Filho, Analyst 139 (2014) 2842.
[28] S. Reddy, B.E.K. Swamy, H. Jayadevappa, Electrochim. Acta 61 (2012) 78.
[29] J. Yang, L.C. Jiang, W.D. Zhang, S. Guanasekaran, Talanta 82 (2010) 25.
[30] M. Multi, A. Erdem, A. Caliskan, A. Sinag, T. Yumak, Colloids Surf. B 86 (2011) 154.
[31] V. Cesarino, I. Cesarino, F.C. Moraes, S.A.S. Machado, L.H. Mascaro, J. Braz. Chem. Soc. 25 (2014) 502.
[32] H. Chena, Z. Zhanga, R. Caia, W. Raoa, F. Long, Electrochim. Acta 117 (2014) 385.
[33] L. Luo, F. Li, L. Zhu, Y. Ding, Z. Zhang, D. Deng, B. Lu, Colloids and Surfaces B 102 (2013) 307.
[34] Z. Wu, Y. Wang, L. Sun, Y. Mao, M. Wang, C. Lin, J. Mater. Chem. A 2 (2014) 8223.
[35] S.I. Hashemi, B. Fazelabdolabadi, S. Moradi, A.M. Rashidi, A. Shahrabad, H. Bagherzadeh, Appl Nanosci (2015) 1.
[36] Y.B.M. Mahaleh, S.K. Sadrnezhaad, D. Hosseini, J. of Nanomaterials (2008) 1.
[37] L.A. Saghatforoush, M. Hasanzadeh, S. Sanati, R. Mehdizadeh, Bull. Korean Chem. Soc. 33 (2012) 2613.
[38] B. Liu, L. Luo, Y. Ding, X. Si, Y. Wei, X. Ouyang, D. Xu, Electrochim. Acta 142 (2014) 336.
[39] Analytical Methods Committee,, Recomendations for the definition, estimation and use of the detection limit, Analyst 112 (1987) 199.
[40] F.C. Moraes, M.F. Cabral, L.H. Mascaro, S.A.S. Machado, Surf. Science 605 (2011) 435.
[41] H. Long, T. Shi, H. Hu, S. Jiang, S. Xi, Z. Tang, Scientific Reports 7413 (2014) 1.
[42] L.G. Teoh, K. Li, Materials Transactions 12 (2012) 2135.
[43] J.Y. Lee, K. Liang, K.H. An, Y. Lee, Synthetic Metals 150 (2005) 153.
[44] L.A. Goulart, F.C. Moraes, L.H. Mascaro, Materials Science and Engineering C 58 (2016) 768.
[45] Y. Yao, Y. Wen, J. Xu, L. Zhang, X. Duan, L. Lu, H. Xia, Monatsh Chem 145 (2014) 137.
[46] S.M. Silva, F.M. Oliveira, D.D. Justino, L.T. Kubota, A.A. Tanaka, F.S. Damos, R.C.S. Luz, Electroanalysis 26 (2014) 602.
[47] H.S. Han, J. You, H. Seol, H. Jeong, S. Jeon, Sensors and Actuators B 194 (2014) 460.
[48] Y. Yao, Y. Wen, J. Xu, L. Zhang, X. Duan, L. Lu, H. Xia, Monatsh Chem 145 (2014) 137.
[49] Q. Guo, J. Huang, P. Chen, Y. Liu, H. Hou, T. You, Sensors and Actuators B 163 (2012) 179.
[50] D. Zhao, X. Zhang, L. Feng, L. Jia, S. Wang, Colloids and Surfaces B: Biointerfaces 74 (2009) 317.
[51] H. Du, J. Ye, J. Zhang, X. Huang, C. Yu, J. of electroanal. chemistry 650 (2011) 209.
[52] S. Poorahong, C. Thammakhet, P. Thavarungkul, W. Limbut, A. Numnuam, P. Kanatharana, Microchim Acta 176 (2012) 91.
[53] X. Tu, L. Yan, X. Luo, S. Luo, Q. Xie, Electroanalysis 21 (2009) 2491.
[54] Y. Lina, K. Liua, C. Liua, L. Yina, Q. Kanga, L. Lia, B. Li, Electrochimica Acta 133 (2014) 492.
[55] M. Portaccio, D. Di Tuoro, F. Arduini, M. Lepore, D.G. Mita, N. Diano, L. Mita, D. Moscone, Biosensors and Bioelectronics 25 (2010) 2003.